BIOCHEMISTRY
including biophysical chemistry & molecular biology

Article

pubs.acs.org/biochemistry

FTDP-17 Tau Mutations Induce Distinct Effects on Aggregation and Microtubule Interactions

Benjamin Combs and T. Chris Gamblin*

Department of Molecular Biosciences, University of Kansas, 1200 Sunnyside Avenue, Lawrence, Kansas 66045, United States

Supporting Information

ABSTRACT: FTDP-17 mutations in the tau gene lead to early onset frontotemporal dementias characterized by the pathological aggregation of the microtubule-associated protein tau. Tau aggregation is closely correlated with the progression and severity of localized atrophy of certain regions in the brain. These mutations are primarily located in or near the microtubule-binding repeat regions of tau and can have vastly different effects on the protein. Some mutations have been linked to effects such as increased levels of aggregation, hyperphosphorylation, defects in mRNA splicing, and weakened interaction with microtubules. Given the differential effects of the mutations, it may not be surprising that the pathology associated with FTDP-17 can vary widely as well. Despite this variety, several of the mutations are commonly used interchangeably as aggregation inducers for in vitro and in vivo models of tauopathies. We generated recombinant forms of 12 FTDP-17 mutations chosen for their predicted effects on the charge, hydrophobicity, and secondary structure of the protein. We then examined the effects that the mutations had on the properties of in vitro aggregation of the protein and its ability to stabilize microtubule assembly. The group of mutations induced very different effects on the total amount of aggregation, the kinetics of aggregation, and filament morphology. Several of the mutations inhibited the microtubule stabilization ability of tau, while others had very little effect compared to wild-type tau. These results indicate that the mechanisms of disease progression may differ among FTDP-17 mutations and that the effects of the varying mutations may not be equal in all model systems.

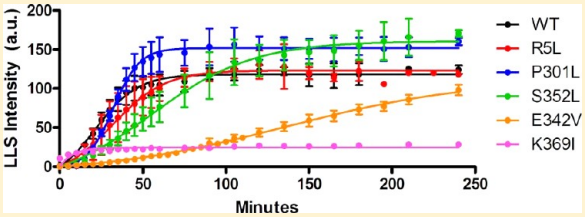

Tauopathies are a group of neurodegenerative disorders characterized by the pathological aggregation of the microtubule-associated protein tau. Although tau can be found in a variety of tissues, it is predominantly found in neurons where its primary functions are to promote the assembly and stability of microtubules and to interact with cellular membranes and play a role in regulation of microtubule spacing as well as axonal transport.[1−5] The tau gene contains 16 exons that, in the central nervous system, give rise to six distinct isoforms that differ by their pattern of inclusion or exclusion of exons 2, 3, and 10. Exon 10 encodes one of four potential microtubule-binding repeat regions (MTBRs) that are the primary source of interactions of tau with microtubules. Each MTBR contains a highly conserved 18-amino acid repeat and an inter-repeat regions of 13 or 14 amino acids, both of which make significant contributions to microtubule binding.[6−8]

Tau MTBRs were found to comprise the core of pathologically aggregated tau filaments[9] and have been found to be necessary and sufficient for the aggregation of tau into straight and paired helical filaments.[10,11] Within the MTBR, the sequences ^{275}VQIINK in exon 10 and ^{306}VQIVYK in exon 11 misfold into β-strands that subsequently interact with adjacent tau molecules to form characteristic amyloid structure.[11−15] The nucleation step, formation of oligomers, is likely the first step in tau aggregation and can be followed by a slower elongation phase that leads to the formation of longer straight or paired helical filaments from these oligomers.[16,17] Aggregated tau then accumulates in pathological structures such as neurofibrillary tangles, neuropil threads, Pick bodies, and others that correlate with the type and severity of clinical impairment in neurodegenerative tauopathies (reviewed in refs 18 and 19).

In Alzheimer's disease and other related tauopathies, tau aggregation is oftentimes associated with other pathological structures such as β-amyloid extracellular senile plaques. It was therefore unclear whether tau aggregation played a role as a causative agent in neuronal cell death or was simply a byproduct of other toxic mechanisms. The potential for a causative role was greatly strengthened with the identification of a group of mutations in the tau gene that led to early onset frontotemporal dementias.[20,21] Many of the mutations cause increased propensities for aggregation and weakened microtubule interactions that could represent toxic gain and loss of functions, respectively.[13,22−31] Several of the mutations have also been utilized in a diverse set of model organisms, including nematodes, flies, *Xenopus*, and mice (refs 25 and 32−35; reviewed in ref 36). These naturally occurring mutations have provided an invaluable tool for the study of tau aggregation, but their effects have not always been consistent across the spectrum of mutants or model organisms.[37]

Received: August 10, 2012
Revised: October 5, 2012
Published: October 8, 2012

   dx.doi.org/10.1021/bi3010818 | *Biochemistry* 2012, 51, 8597−8607

It is possible that some of the observed differences in the effects of tau aggregation in cellular and animal models are a direct result of the various FTDP-17 mutations employed to generate aggregated tau. Certain FTDP-17 mutations have been shown to increase the rate or total amount of tau aggregation both in vitro and in vivo, which may be leading to early onset tauopathies;[22,26,34,38,39] some FTDP-17 mutants exhibit a decreased level of binding to microtubules and an impaired ability to stabilize polymerization of tubulin, while others have little effect.[23,40] In addition, the progression and pathologies of FTDP-17 can vary greatly depending on the specific mutation, indicating that initial causes of the disease may vary as well (reviewed in ref 41). We therefore sought to compare several FTDP-17 mutations under the same conditions to determine how they affected aggregation and microtubule interaction, two factors that may have causative roles in the toxicity of these diseases, and whether differences in the intrinsic effects of FTDP-17 mutations could be correlated to these changes. From the 25 known FTDP-17 missense mutants of tau, we chose to model the 12 mutations predicted to have the most significant impact on tau charge, hydrophobicity,[42] and structure.[43] Our predictions were based on an analysis demonstrating that these parameters were the primary determinants of aggregation rates.[44] We chose to model these mutants in the background of full-length 2N4R tau in vitro to provide direct side-by-side comparisons to assess the impact of the structural modifications.

We found that the FTDP-17 mutants had very different effects on the aggregation and microtubule interactions of tau. These changes in aggregate amounts, rates, and morphologies could help in our understanding of the varied pathologies and toxicities resulting from the mutations. While some of the mutations had similar effects on tau function and aggregation, we found that there was not a simple correlation between the effects on tau and the protein's charge, hydrophobicity, or predicted structure. This indicates that predictive methods are insufficient for determining the impact of tau mutations on the severity of impairment.

EXPERIMENTAL PROCEDURES

Selection of FTDP-17 Mutations. Mutations were selected on the basis of their predicted effects on average hydrophobicity, charge, α-helical structure, β-strand structure, and turns. These predictions were calculated across seven-amino acid sequences for the entire 2N4R tau isoform using Kyte−Doolitte values to estimate hydrophobicity[42] and Chou−Fassmann parameters for effects on secondary structure.[43] The effect of each mutant was ranked according to each of these factors, and the total effect was estimated on the basis of summation of rankings for each variant. The 11 mutants predicted to have the largest effects on the structure of the protein were chosen along with V337M, a mutant commonly used to generate tau aggregation in in vivo models.

Protein Expression and Purification. All wild-type (WT) and FTDP-17 mutant proteins were expressed and purified as described previously.[45] The FTDP-17 mutations were created using the Quikchange site-directed mutagenesis kit from Stratagene (La Jolla, CA). The following mutations were generated in a full-length 2N4R tau background contained in a pT7C vector: R5L, G272V, ΔN296, P301L, G303V, L315R, S320F, V337M, E342V, S352L, K369I, and G389R.

Arachidonic Acid-Induced Polymerization. Recombinant WT and mutant tau protein, at a concentration of 2 μM, was incubated in buffer containing 0.1 mM EDTA, 5 mM dithiothreitol, 10 mM Hepes buffer (pH 7.64), 100 mM NaCl, and 3.75% ethanol in a 1.5 mL microcentrifuge tube. The polymerization inducer molecule was arachidonic acid (ARA) at a concentration of 75 μM. Reactions were allowed to proceed overnight at 25 °C.

Thioflavin S Fluorescence. The total amount of aggregation was measured utilizing the binding of thioflavin S (ThS) from Sigma-Aldrich (St. Louis, MO); 150 μL of each reaction mixture was added to separate wells in a 96-well, white, flat-bottom plate. ThS was diluted in water and added to the well to a final concentration of 20 μM. The fluorescence shift was measured by using a Cary Eclipse fluorescence spectrophotometer (Varian Analytical Instruments, Walnut Valley, CA) with an excitation wavelength of 440 nm and an emission wavelength of 520 nm. The PMT voltage was set to 650 V. Readings from a reaction with 2 μM protein and 0 μM ARA were used as a blank and subtracted from the reading for each reaction.[45]

Right-Angle Laser Light Scattering. Aggregation of the protein was also read by adding 180 μL of the reaction mixture to a 5 mm × 5 mm optical glass fluorometer cuvette (Starna Cells, Atascadero, CA). A 12 mW solid state laser, with a wavelength (λ) of 532 nm and operating at 7.6 mW, was aimed at the cuvette. The amount of light scattered by particles in the reaction mixture was measured by capturing the amount of light perpendicular to the angle of the beam using a Sony XC-ST270 digital camera. The images were captured at varying aperture settings (from f4 to f11) and analyzed using the histogram function of Adobe Photoshop CS5 version 12.0.1.[25]

ARA-Induced Polymerization Kinetics. ARA was added to our polymerization buffer [0.1 mM EDTA, 5 mM dithiothreitol, 10 mM Hepes buffer (pH 7.64), and 100 mM NaCl] to a final concentration of 75 μM and 3.75% ethanol in a 5 mm × 5 mm optical glass fluorometer cuvette. Tau polymerization was measured by collecting images of the right-angle scattered light at specific time points beginning from the initiation of the reaction upon addition of protein, at a final concentration of 2 μM, to the ending once the reaction had reached a steady state. The data were fit to the Finke−Watzky two-step mechanism, designed to describe the nucleation and elongation of protein aggregation.[46] The mechanism assumes simplified nucleation ($A \xrightarrow{k_1} B$) and elongation ($A + B \xrightarrow{k_2} 2B$) steps to yield the following equation:

$$[B]_t = [A]_0 - \frac{\frac{k_1}{k_2} + [A]_0}{1 + \frac{k_1}{k_2[A]_0}\exp(k_1 + k_2[A]_0)t}$$

The k_1 and k_2 rate constants are used to qualitatively compare the rates of nucleation and elongation, respectively, of our protein aggregation reactions.

Transmission Electron Microscopy. The ARA-induced polymerization reaction mixtures were diluted 1:10 in polymerization buffer and 2% glutaraldehyde. After a 5 min incubation, a Formvar-coated copper grid (Electron Microscopy Sciences, Hatfield, PA) was placed on top of a 10 μL drop of the diluted sample for 1 min. The grid was then blotted on filter paper, placed on a drop of water, blotted with filter paper, placed on a drop of 2% uranyl acetate, and blotted dry. The grid was then placed on another drop of 2% uranyl acetate for 1 min and blotted dry for a final time. For all tau variants, a single grid was prepared and examined from each of three separate reactions.

The grids were examined using a TECNAI G^2 20 electron microscope (FEI Co., Hillsboro, OR). Images were collected with the Gatan Digital Micrograph imaging system at a magnification of 3600×. Five images were collected from each grid and analyzed. The aggregated tau in each of the 15 images was quantified by using Image-Pro Plus 6.0. The macro was designed to recognize filaments with a total perimeter of >30 nm. This captured what we felt to be legitimate aggregates while eliminating background noise. The perimeter of each filament was measured and divided by 2 to estimate the filament's length. These values were totaled to estimate the total amount of aggregated material in each image. The total polymerization per image was calculated by taking the mean of all total polymerization values. The mean of all filament lengths was also determined by calculating the mean length of all filaments in a given image and is reported as a mean of those values with the error bars representing the standard deviation.

Tubulin Polymerization Assay. The tubulin polymerization assay kit from Cytoskeleton, Inc. (Denver, CO), was used to measure the polymerization of tubulin. The reaction conditions included WT tau or one of the tau variants at 1 μM, or a control compound, added along with 1 mM GTP, 2 mg/mL (~36 μM dimerized) tubulin, 2 mM $MgCl_2$, and 0.5 mM EGTA in 80 mM PIPES buffer (pH 6.9). The reaction proceeded in a black, flat-bottom polystyrene 96-well plate. Paclitaxel was used at 3 μM in one reaction to serve as a positive control for tubulin polymerization, as well as a way to normalize separate reactions. One well contained no additional compound as a negative control. After addition of the compounds, the plate was inserted into a FlexStation II Fluorometer (Molecular Devices Corp., Sunnyvale, CA) set at a temperature of 37 °C, and the reaction mixtures were shaken for 5 s. The fluorescence was measured with an excitation wavelength of 355 nm and an emission wavelength at 455 nm at 1 min intervals for 1 h. The data were fit to the Gompertz equation as described previously.[47,48]

$$y = ae^{-e^{-t-t_i/b}}$$

where a is the maximal amount of tubulin polymerization, $t_i - b$ is the lag time from reaction initiation to the start of polymerization, and k_{app}, or $1/b$, is proportional to the rate of polymerization.

Statistical Analysis. An unpaired two-tailed Student's t test was used to compare means of WT values to mean values of each mutant for thioflavin S fluorescence, right-angle laser light scattering, quantitative electron microscopy, and kinetics parameters. A paired two-tailed t test was used to compare the values for the microtubule assembly assay. p values of ≤ 0.05 are denoted with one asterisk, ≤ 0.01 with two asterisks, and ≤ 0.001 with three asterisks. Because variation among the mutants is also important to consider, statistical variation in the whole groups was measured by using a one-way analysis of variance (ANOVA) with a Tukey's multiple-comparison test and compiled in tables included as Supporting Information. The p values for this comparison are also denoted using the asterisk system described above.

RESULTS

Selection of FTDP-17 Mutations. A list of 25 known FTDP-17 mutations was generated and ranked on the basis of the total predicted changes to the structure of the protein. The 11 mutations predicted to induce the largest structural changes were selected along with V337M, which was selected because it has previously been used in several model organisms. The majority of the chosen FTDP-17 mutations can be found within, or very close to, one of the four MTBRs, while the R5L and G389R mutations are found in the N- and C-terminal regions, respectively (Figure 1).

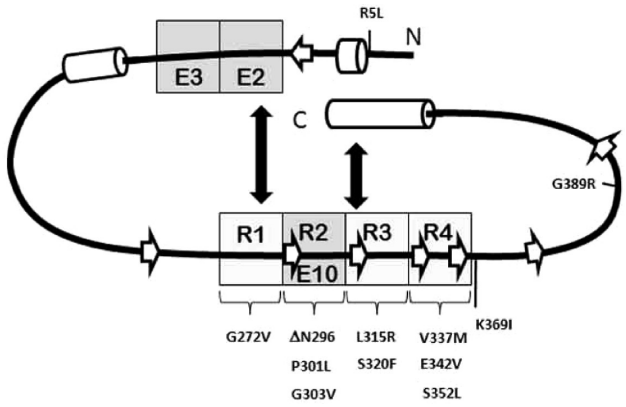

Figure 1. Schematic of FTDP-17 mutations in 2N4R tau. Each of the naturally occurring FTDP-17 mutations indicated in the figure was created in a full-length 2N4R tau background. E2, E3, and E10 represent exons that can be excluded from other tau isoforms. Regions known to exhibit transient secondary structure are represented by cylinders (α-helices) or arrows (β-strands). Boxes R1−R4 represent microtubule-binding repeat regions.

FTDP-17 Mutations Induce Varying Effects on Total Polymerization. In vitro experiments were used to examine the effects of the 12 mutations on the ARA-induced polymerization of tau at 2 μM protein and 75 μM ARA.[49] After the reactions had proceeded overnight, the total amount of aggregation was measured by ThS fluorescence and right-angle laser light scattering (LLS). Half of the mutant proteins displayed an increase in ThS fluorescence compared to that of WT tau protein (G272V, P301L, G303V, S320F, S352L and G389R), indicating that more protein had polymerized in those reactions. Others had levels of polymerization that were similar to that of WT tau (R5L, ΔN296, V337M, and E342V), while two of the mutants showed a clear decrease (L315R and K369I) (Figure 2A).

LLS can be used as another method to measure relative amounts of protein aggregation.[25] However, in this case, the results differed from those found with ThS fluorescence. Only three mutants showed a clear increase over WT (R5L, P301L, and S352L); five of the mutants showed a decrease in scattered light (G272V, G303V, L315R, S320F, and K369I), and four mutants had levels similar to that of WT (ΔN296, V337M, E342V, and G389R) (Figure 2B). Results from one-way ANOVAs with Tukey's multiple-comparison tests can be found in Tables S1 and S2 of the Supporting Information. This analysis demonstrates not only that many of the mutants are different from WT but also that a wide range in variation exists between mutants.

FTDP-17 Mutations Induce Varying Effects on Aggregate Morphology. Because LLS is known to be affected by the length distribution of the aggregates[25] and the structure of tau recognized by ThS is unknown,[16,50] the aggregates of tau were viewed directly by electron microscopy (Figure 3). Direct visualization of the aggregates can help in elucidating some causes of the apparent variation between the

dx.doi.org/10.1021/bi3010818 | Biochemistry 2012, 51, 8597−8607

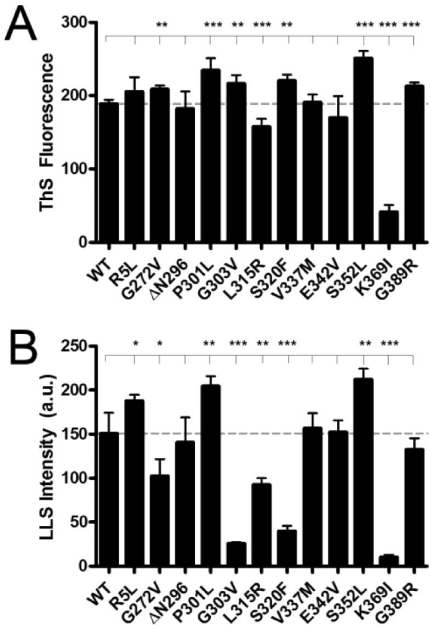

Figure 2. Polymerization of wild-type and FTDP-17 mutant tau measured by thioflavin S staining and right-angle laser light scattering. Polymerization reaction mixtures contained WT or one of 12 FTDP-17 mutant versions of tau (each at 2 μM) and 75 μM ARA. Reaction mixtures were incubated overnight at 25 °C. The final extent of polymerization was measured by (A) ThS fluorescence and (B) right-angle LLS as described in Experimental Procedures. Data represent the mean from three experiments ± the standard deviation. Asterisks represent p values from Student's unpaired t tests comparing means from each mutant to that of WT: $p < 0.05$ (one asterisk), $p < 0.01$ (two asterisks), and $p < 0.001$ (three asterisks). More extensive statistical analysis can be found in the Supporting Information.

ThS and LLS results (Figure 2). WT tau displays a characteristic mixture of longer filaments and smaller aggregates less than 100 nm in length, hereafter described as oligomers (Figure 3A). Examination of the images made it abundantly clear that the mutations were inducing very different effects on the aggregation of the protein. Some of the mutants, such as G303V and S320F, consist almost entirely of oligomers (Figure 3F,H). Others, including R5L, S352L, and P301L, seem to be lacking oligomers and display longer filaments than WT tau (Figure 3B,E,K). Very few aggregates were associated with K369I, which confirms earlier ThS and LLS results (Figures 2 and 3L). We next sought to determine if the apparent differences we observed could be detected by quantitative methods and whether these differences were significant. To accomplish this, we measured the number and length of filaments displayed in five representative images from each of three different reactions for each tau variant.

Quantitation of the total amount of aggregated material indicated that most of mutant forms of tau variants polymerized to an extent similar to that of WT tau, but images from G303V, S320F, and E342V all contained more total polymerized tau than WT (Figure 4A). In contrast, K369I and G389R displayed less polymerization than WT in these images. K369I had considerably fewer aggregates than WT, and these aggregates were very short in nature and in general did not stain as intensely as tau aggregates associated with WT and the other mutants, again indicating low levels of polymerization (Figures 3L and 4B).

The differences in aggregation, apparent in Figure 3, were confirmed by comparing the average lengths of all filaments for each tau variant. Several mutants (G272V, G303V, L315R, S320F, and G389R) exhibited shorter average filament lengths, while filaments from R5L, P301L, and S352L were much longer on average than WT (Figure 4B). Average filament lengths are not amenable to statistical analysis because of their exponential distribution. Therefore, the data from each of the 15 electron micrographs were plotted as average filament length versus the number of filaments formed to demonstrate the variation in the data (Figure S1 of the Supporting Information). These plots also supported the differences in filament morphology described above. Further variation can be observed by determining how much of the total polymerization is due to very short filaments. We calculated the percent of the total polymerized material that consisted of <100 nm filaments (Figure 4C). Approximately 30% of polymerized WT tau was contained in short filaments, while oligomers made up >90% of the total for G303V, S320F, and K369I. Others, such as R5L, ΔN296, P301L, and S352L, again induced a very different effect and contained much lower percentages, indicating that longer filament lengths and fewer oligomers were present (Figure 4C).

In light of the quantitative EM data, the discrepancy between ThS fluorescence and LLS measurements of tau mutant aggregation is likely due to the disparate morphologies of the resulting filaments. In fact, there is a direct correlation between filament length, as measured by electron microscopy (Figures 3 and 4B), and the ratio of ThS fluorescence to LLS values (Figure S2 of the Supporting Information). Therefore, the amount of light scattering from two populations of filaments of very different length distributions may not be equally proportional to the mass of filaments.

The Kinetics of Polymerization Varies by FTDP-17 Mutant. Because the morphology of tau aggregates can be influenced by the rate of polymerization,[49] we sought to determine whether the mutations were affecting the kinetics of polymerization. Polymerization reactions for each mutant were followed by LLS and were then fit to a two-step model of polymerization to determine nucleation and elongation rates (Figure 5). The K369I mutant had nearly undetectable levels of polymerization in this assay and could therefore not be fit to the model.

A visual inspection of the curves indicated a wide range of polymerization kinetics between mutants (Figure 5). A comparison of nucleation rates [k_1 (Figure 6A)] indicated that G272V, G303V, L315R, and S320F had nucleation rates that were significantly increased compared to that of WT, while R5L, P301L, E342V, and S352L had significantly decreased nucleation rates (Figure 6A). G303V, L315R, and S320F also had elongation rates greatly reduced compared to that of WT [k_2 (Figure 6B)], such that the elongation phase was essentially undetectable. E342V and S352L had elongation rates that were significantly reduced compared to that of WT, but elongation was still detectable (Figure 6B). The only mutant with a faster elongation rate than WT was P301L (Figure 6B). In addition to these differences from WT protein, further analysis of the data using one-way ANOVA with Tukey's multiple-comparison tests demonstrates that many of the mutants are significantly different from one another. For example, the kinetics of elongation (k_2) of the P301L mutant is significantly different from those of G303V, L315R, S320F, V337M, S352L, and G389R (Tables S3 and S4 of the Supporting Information).

dx.doi.org/10.1021/bi3010818 | *Biochemistry* 2012, 51, 8597−8607

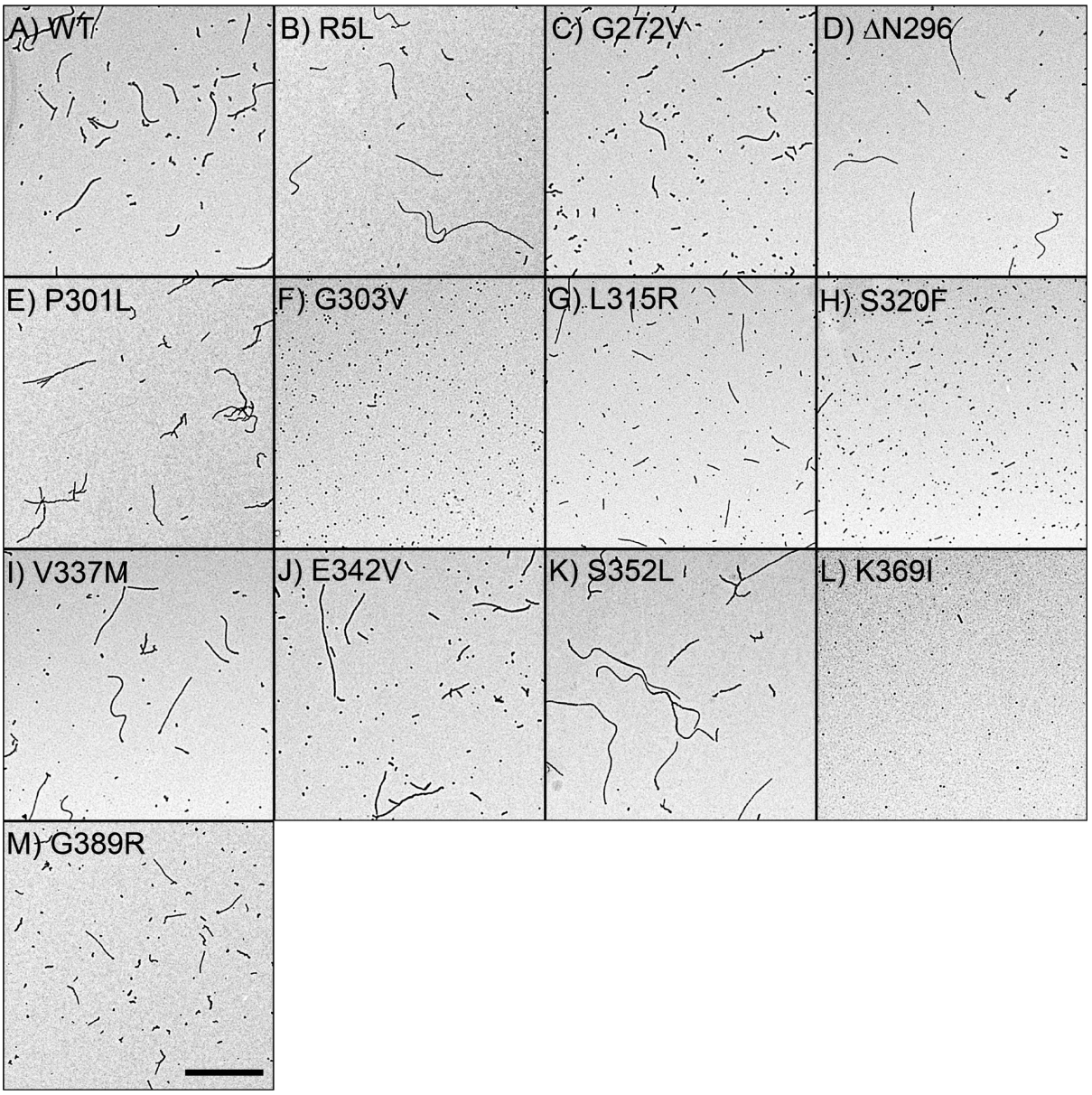

Figure 3. Electron micrographs of polymerization reaction mixtures containing 2 μM protein and 75 μM ARA. Representative electron micrographs for (A) WT tau, (B) R5L, (C) G272V, (D) ΔN296, (E) P301L, (F) G303V, (G) L315R, (H) S320F, (I) V337M, (J) E342V, (K) S352L, (L) K369I, and (M) G389R. The scale bar in panel M represents 1 μm and is applicable for all images.

FTDP-17 Mutations Can Inhibit the Ability of Tau To Stabilize Microtubule Assembly or Have Little Effect. We then sought to determine whether the FTDP-17 mutations would have differential effects on one of tau's normal functions of stabilizing microtubules. Microtubule polymerization was monitored using a fluorescence-based assay, and the resulting curves (Figure 3 of the Supporting Information) were fit to a Gompertz function to determine the maximal extent of microtubule polymerization, the rate of elongation, and the lag time in the presence of the FTDP-17 mutants (Figure 7). Most proteins stabilized microtubules to levels similar to that of WT tau, but G303V, L315R, and S352L did not (Figure 7A). P301L, G303V, S320F, and S352L induced microtubule elongation at a slower rate, while V337M and E342V actually increased the rate of tubulin polymerization (Figure 7B). The lag time for tubulin polymerization was decreased in the presence of G272V, L315R, V337M, E342V, and G389R but increased in the presence of G303V and S352L (Figure 7C). In addition to these differences in FTDP-17 mutants versus WT, results from one-way ANOVAs with Tukey's multiple-comparison tests demonstrate that there were many statistically significant differences between FTDP-17 mutants, as well (Tables S5−S7 of the Supporting Information).

■ DISCUSSION

FTDP-17 mutations in tau are extremely rare but play a particularly important role in the study of tau aggregation associated with familial and sporadic tauopathies. Some of these mutations are commonly used in disease models to enhance protein aggregation. However, among the FTDP-17 mutants, significant variability in symptoms and pathology of diseases exists, indicating that there may be differing root causes of the disease. While most known mutations are found within one of the four MTBRs, the locations vary from the N- to C-terminal

dx.doi.org/10.1021/bi3010818 | *Biochemistry* 2012, 51, 8597−8607

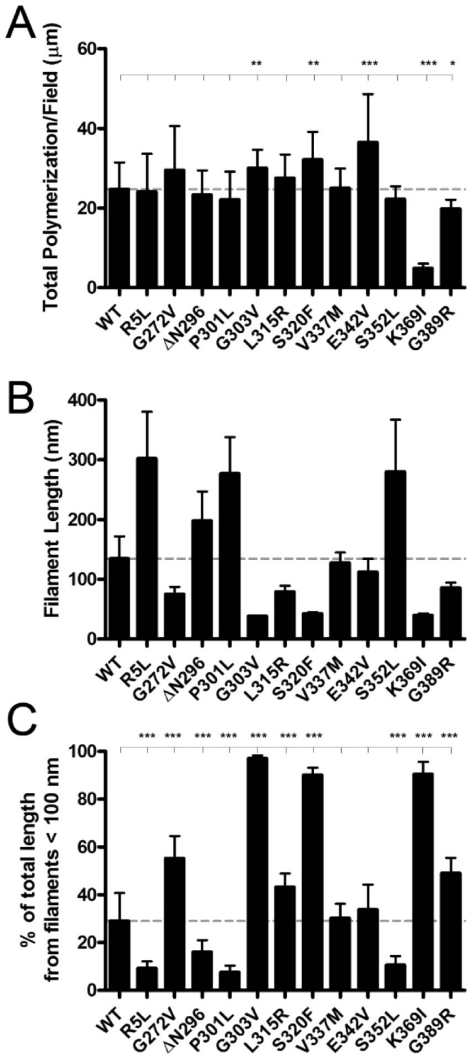

Figure 4. Quantitation of polymerized tau protein in electron micrographs. Images in the electron micrographs from Figure 3 were quantified using Image-Pro Plus 6.0 as described in Experimental Procedures. The graphs display (A) the mean of the total length (micrometers) of polymerized tau filaments per image, (B) the mean length of filaments (nanometers), and (C) the percent of the total length coming from <100 nm filaments for each of the tau variants. Data in panel A represent the means of five images from each of three separate reactions ± the standard deviation (n = 15). Data in panel B represent the means of the mean filament length for each of the 15 images ± the standard deviation. Data in panel C represent the means of the sum of all filament lengths of <100 nm as a percent of the total length for each image ± the standard deviation (n = 15). Asterisks represent p values from Student's unpaired t tests comparing means from each mutant to that of WT: $p < 0.05$ (one asterisk), $p < 0.01$ (two asterisks), and $p < 0.001$ (three asterisks).

regions. The amino acid substitutions or deletions result in increased or decreased hydrophobicity and charge and induce a variety of potential changes in the transient secondary structure of the protein. In addition, other factors such as alterations in splicing or phosphorylation pattern could be playing a major role in the neurodegenerative process.

Because of the differences in the pathology of aggregation and disease progression, it is important to determine how the mutations are changing the properties of the tau protein as well as how these changes could be affecting the associated neurodegeneration patterns. Previous work has shown that the rate of aggregation of tau into amyloid could be predicted by calculating the expected changes in hydrophobicity, charge, and secondary structure due to three known FTDP-17 mutations.[44] In addition, other studies have examined the in vitro properties of small numbers of known mutants.[22,25,26] We sought to directly compare the aggregation and function of WT and a wider variety of FTDP-17 mutant forms of tau under similar conditions, using the same mechanisms for inducing aggregation, and to determine whether these predictive tools would apply to an expanded field of mutations.

After studying the effects of FTDP-17 mutations on the in vitro aggregation of tau and its microtubule stabilization properties, we determined that the mutants had profiles very distinct from that of WT tau as well as each other. We were able to group some of the mutants together on the basis of their common properties and speculate about some of the causes for these general trends, although we could not detect a clear pattern between the effects in these assays and the intrinsic changes predicted to occur due to mutations. Some of the mutations induced similar effects on filament morphology that may be tied to their aggregation kinetics, but the overall trends pointed to large differences in the behavior of the mutated versions of tau in our assays.

Several of the mutants displayed shorter average filament lengths than WT, which seemed to be due to an increase in the number of oligomers and a decrease in the length and number of longer filaments. The increase in the number of oligomers from this group may be explained by the increased rate of nucleation that was also associated with these four mutations. Fast nucleation would take up large amounts of monomeric tau quickly and decrease the protein level below the critical concentration of aggregation before elongation could begin. Interestingly, four of the mutations with decreased filament lengths occur directly before and after the ^{275}VQIINK and ^{306}VQIVYK sequences, important for aggregation of tau, and may be causing increased levels of nucleation through enhancements of the β-strand character.[11,51] G272V, G303V, and S320F are predicted to enhance β-strand structure, and extension of the β-strands in these regions has been shown to enhance polymerization in other mutants, although with slightly different effects.[52] The fourth mutation, L315R, is not predicted to enhance β-strand character, but it would replace a hydrophobic amino acid with a positive charge on the polar and/or charged side of an amphipathic β-strand, which may help promote the cross-β-amyloid structure.[52] Strengthening the β-strand secondary structure in these key regions may increase the level of nucleation, making it more likely that tau will begin to aggregate and leaving little tau left for the elongation phase of polymerization. Therefore, the rate of nucleation is an important determinant of the ratio of oligomers to fibrils formed under these conditions.

Another group of mutations induced the opposite effects on the filament morphology phenotype. R5L, P301L, and S352L all induced fewer, but longer, filaments than WT or the other mutant versions of tau. These were slower to nucleate than WT tau, which could be another indication of the importance of nucleation rate on filament morphology. Despite the similarities in the rates of nucleation, the elongation rates of these three tau mutants varied widely compared to that of WT; R5L was similar, P301L faster, and S352L slower. Even though each of these mutants aggregated into long filaments with few oligomers, the mechanisms of aggregation were quite dissimilar.

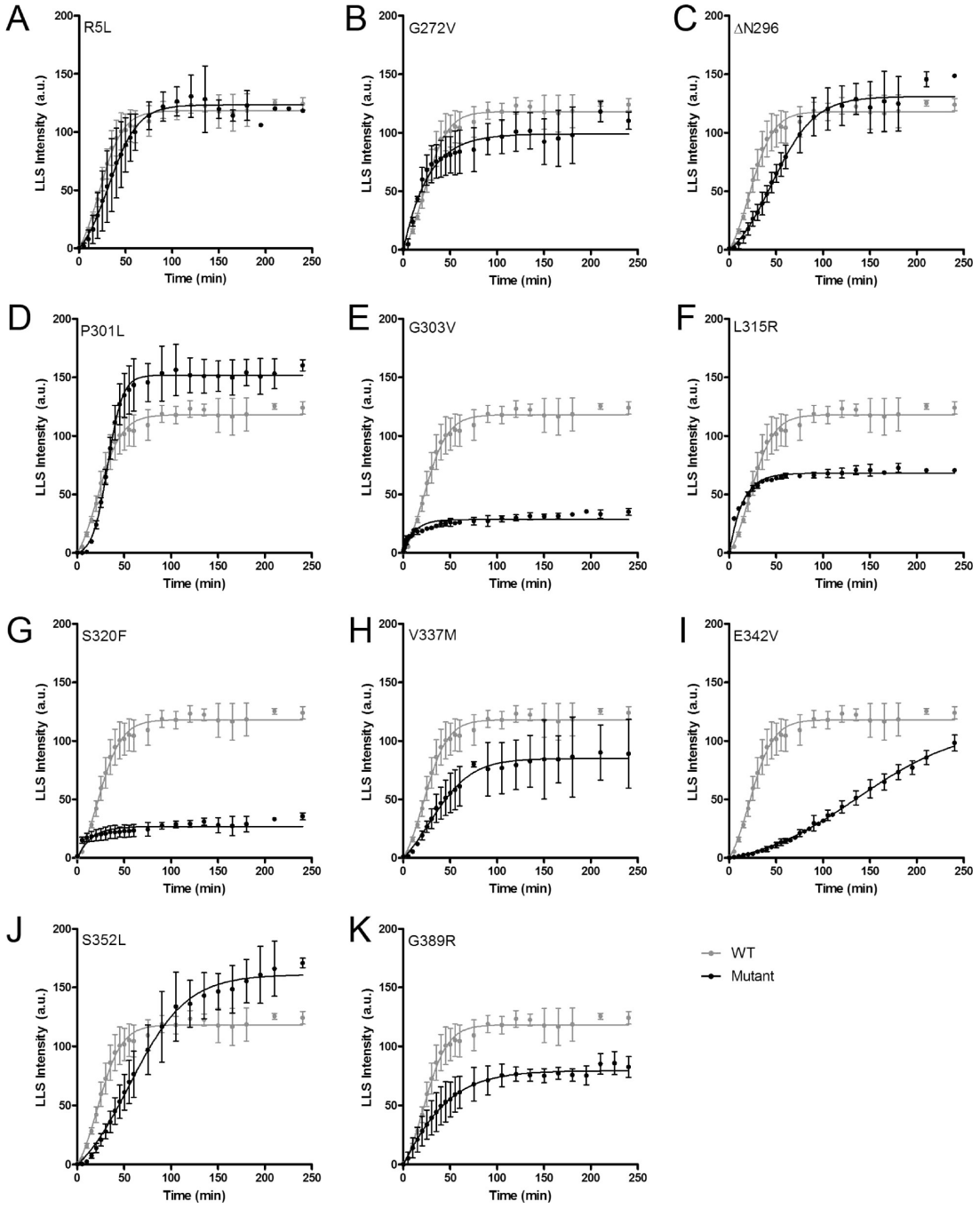

Figure 5. Kinetics of tau polymerization. Polymerization reaction mixtures containing 2 μM tau were initiated by the addition of 75 μM ARA. LLS readings were measured at specific time intervals until the reactions reached a steady state. The traces here represent mean values ± the standard deviation from three reactions fit to the Finke–Watzky mechanism described in Experimental Procedures and displayed over 250 min for WT tau protein (light gray) and various FTDP-17 mutant tau proteins (black), including (A) R5L, (B) G272V, (C) ΔN296, (D) P301L, (E) G303V, (F) L315R, (G) S320F, (H) V337M, (I) E342V, (J) S352L, and (K) G389R.

It may seem unusual that R5L, a mutation that is far from the MTBR, would have such large effects on the aggregation of the protein, but the N-terminal region has been shown to have an enhancing effect on aggregation that may be due to alterations in the global hairpin conformation.[38,53,54] The P301L mutation is much closer to the ^{306}VQIVYK hexapeptide than R5L, and the removal of a proline in the PGGG sequence preceding it could assist in the formation of a β-strand in such a way as to stabilize the formation of longer filaments with an altered morphology.[55] S352L also enhances the β-strand character around the ^{350}VQLKI sequence, which is very similar to the ^{275}VQIINK and ^{306}VQIVYK sequences that form the amphipathic β-strands crucial for the formation of tau filaments. The addition of another amyloidogenic sequence could assist in the stabilization of longer filaments.

While the mutants discussed above had obvious effects on the morphology of the aggregates, other mutants, such as ΔN296, V337M, and E342V, displayed aggregates that were much more similar to WT protein. These mutants aggregated into mixes of short and long filaments with roughly the same

dx.doi.org/10.1021/bi3010818 | *Biochemistry* 2012, 51, 8597–8607

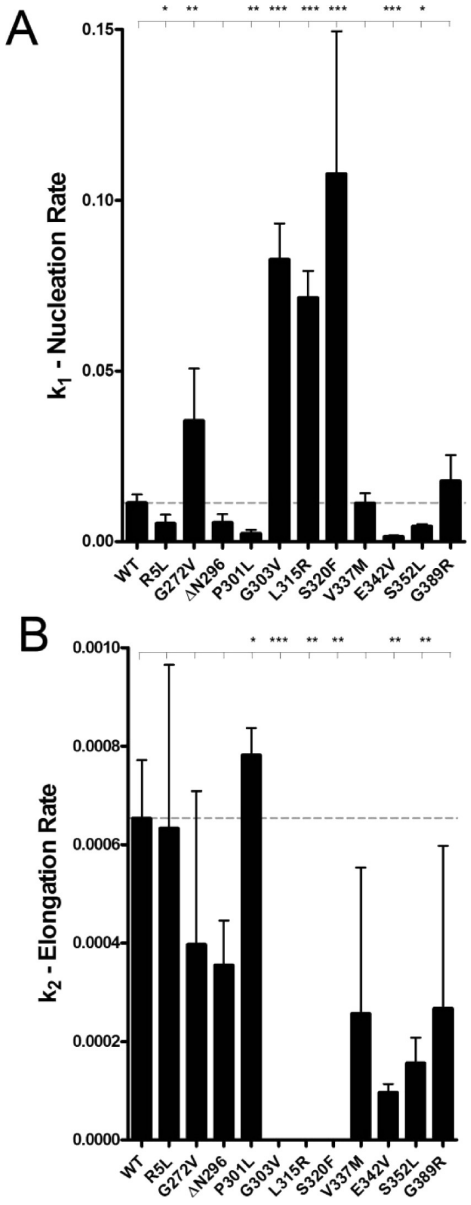

Figure 6. Comparison of tau polymerization kinetics. The parameters describing the tau polymerization kinetics curves fit to the Finke–Watzky mechanism are displayed. The first parameter is (A) k_1, representing the rate of nucleation or formation of oligomers. The second parameter is (B) k_2, the rate of elongation or extension of the oligomeric tau aggregates into filaments. Data represent means of values for fits of at least three separate reactions ± the standard deviation. Asterisks represent p values from Student's unpaired t tests comparing means from each mutant to that of WT: $p < 0.05$ (one asterisk), $p < 0.01$ (two asterisks), and $p < 0.001$ (three asterisks). More extensive statistical analysis can be found in the Supporting Information.

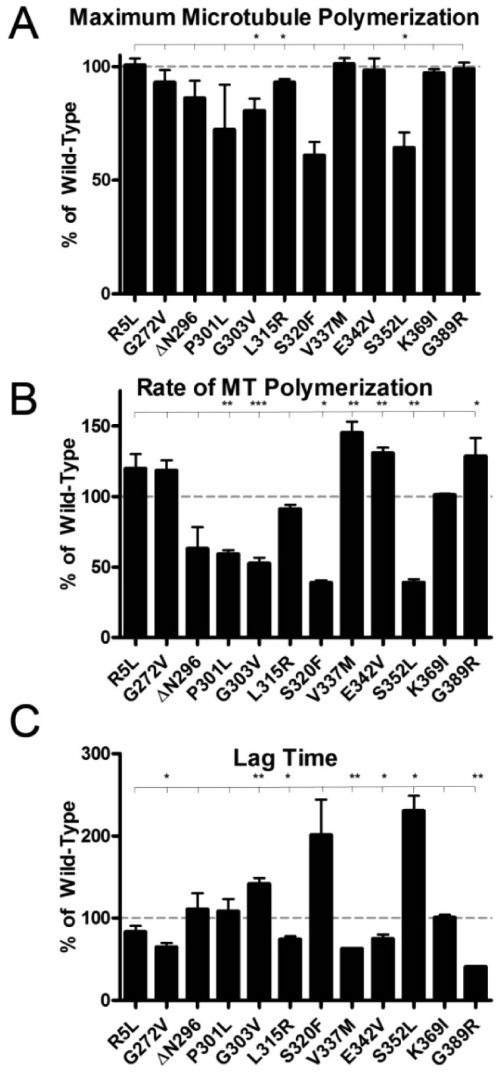

Figure 7. Stabilization of microtubule assembly by tau protein. The tau variants were incubated with tubulin, and its polymerization was measured via a fluorescence assay. Numbers were normalized to values of polymerization in the presence of paclitaxel. The relative fluorescence units (y-axis) were plotted vs time (x-axis) and fit to the Gompertz equation as described in Experimental Procedures. From the parameters describing these curves, the percents of WT values are shown for the (A) maximal amount of microtubule polymerization in the presence of each protein, (B) k_{app} or the rate of microtubule polymerization, and (C) the lag time, the time before microtubule polymerization is detected. These values are means of the percent changes from WT in three separate experiments ± the standard deviation. Asterisks represent p values from Student's paired t tests comparing means from each mutant to that of WT: $p < 0.05$ (one asterisk), $p < 0.01$ (two asterisks), and $p < 0.001$ (three asterisks). More extensive statistical analysis can be found in the Supporting Information.

number of filaments as WT tau. These mutations are farther from the ^{275}VQIINK and ^{306}VQIVYK sequences and may not have equally strong effects on those regions even if they are enhancing the β-strand character around them. These minor changes may indicate that the root causes of these tauopathies may lie somewhere other than direct increases in the level of tau aggregation. For example, the N296 position is also associated with other FTDP-17 mutations that can lead to splicing defects, and V337M can lead to increased levels of phosphorylation[31] (reviewed in ref 56).

While general trends in the aggregation of mutated proteins could be identified, the interactions with microtubules followed an alternate pattern. Only mutations that occur within one of the 18 amino acid repeats in the MTBR displayed effects on the ability of the protein to stabilize the assembly of microtubules, confirming previous results with other FTDP-17 mutations.[57] Of the mutants that fell outside of the MTBR or in one of the

dx.doi.org/10.1021/bi3010818 | Biochemistry 2012, 51, 8597–8607

inter-repeats (R5L, L315R, V337M, E342V, K369I, and G389R), only L315R displayed any decrease in the total amount of microtubule polymerization from that of WT tau. This was a relatively minor change compared to the effects of the other mutants and was in agreement with previous results.[58] All of the mutants located within one of the repeat regions were unable to stabilize the same maximal level of microtubule polymerization, stabilized a slower rate of polymerization, or altered the lag time compared to that of WT tau. These results, combined with the large percentage of FTDP-17 mutations located in a MTBR, indicate that interactions with microtubules may play a key role in the progression of these tauopathies. Further research is needed to determine how altered microtubule interactions may be affecting tau aggregation as well as if affected microtubule dynamics may be playing a more direct role in toxicity.

Direct comparisons of our results to previous studies can be difficult because of the differing experimental setup. The most common differences involve the type of tau aggregation inducer employed, the buffer conditions, and the tau isoform used in the assays. Our data confirm previous results indicating that P301L is a very fast aggregator compared to WT, several of these FTDP-17 mutants have weakened abilities to stabilize the assembly of microtubules and increased levels of aggregation, and K369I typically forms smaller aggregates.[25,59−61] Occasionally, differences were seen in the kinetics of aggregation that may be ascribed to how the data are measured and to what type of curve they are fit. We feel that the Finke−Watzky mechanism is best able to describe the complex process of tau aggregation in a simplified manner and accurately represented differences in the mechanisms of aggregation for the studied mutations.

The fact that significant differences exist in how these mutants aggregate, the types of aggregates that are seen, and their ability to perform normal functions of tau in vitro should not be particularly surprising given the diversity of disease phenotypes associated with FTDP-17 cases and tauopathies in general. Conformational differences among the mutations are likely to affect the protein's aggregation in complex ways that could then have a direct impact on disease progression. These differences could manifest themselves in the initiation, morphology, or spread of aggregation. While the end result may always be aggregation of tau and degeneration of neurons, the mechanisms by which the various diseases reach that point may be drastically different, and alternate therapeutic interventions may be required on the basis of the initiating cause of the disorder. As it is likely that sporadic tauopathies also have different initiating factors, information about how certain FTDP-17 mutations affect tau may be applicable to the progression of those diseases as well.

To attempt to explain some of these initiating factors, we attempted to find correlations between the intrinsic effects of our chosen mutations and their effects on tau in our various assays. However, we were unable to detect any correlations among these components. It is likely that these effects are complicated and dependent on the specific location of the mutation.

Given the importance of the MTBR in the function and dysfunction of tau, it is likely that location is a very important factor for how these mutations are affecting the aggregation of the protein. Mutations that increased the hydrophobicity and β-strand character, especially in the MTBR, seem to increase the rate of nucleation and decrease the average filament length, but exceptions to this also exist. The causes of familial tauopathies are likely quite complex. Mutation-induced effects on the intrinsic properties of tau may alter its propensity for aggregation or the morphology of its aggregates and lead to early onset tauopathies. However, changes in mRNA splicing, interactions with microtubules, or phosphorylation levels could also lead to aggregation of the protein or neuronal death. In addition, the mutations could also affect other properties of the protein, including interactions with protein degradation systems, kinases, or fast axonal transport among others.

Because of the variation in location and effects on intrinsic properties of tau, significant differences exist in how FTDP-17 mutations affect the protein. While these mutations can be quite useful for in vitro and in vivo models of tau aggregation and tauopathies, it may be important to consider the differential effects when comparing results from various model systems. Further work on characterizing these mutations and their effects on in vivo organisms may help explain how the various FTDP-17 mutations are leading to tauopathies and how these mechanisms are affecting our understanding of the progression of sporadic tauopathies.

■ ASSOCIATED CONTENT

Supporting Information

A plot of average filament length and number of filaments for each of the electron micrographs, a graph displaying the correlation between filament length and the ratio of thioflavin S fluorescence to right-angle laser light scattering, a series of graphs displaying the mean values of all microtubule assembly traces, and tables of one-way ANOVA with Tukey's multiple-comparison tests to describe the statistical significance of differences in results between pairs of each tau variant in our assays (ThS, LLS, tau polymerization kinetics, and microtubule assembly assays). This material is available free of charge via the Internet at http://pubs.acs.org.

■ AUTHOR INFORMATION

Corresponding Author

*Department of Molecular Biosciences, University of Kansas, 1200 Sunnyside Ave., Lawrence, Kansas 66045. Telephone: (785) 864-5065. Fax: (785) 864-5321. E-mail: gamblin@ku.edu.

Funding

Support was provided by CurePSP 498-11 (T.C.G.) and National Institutes of Health Grant GM103418 (T.C.G.).

Notes

The authors declare no competing financial interest.

■ ACKNOWLEDGMENTS

We thank Akosua Kernizan, James Odum, Yamini Mutreja, Smita Paranjape, Mike Branden, and Sonia Hall for their assistance in generation of the tau mutants and protein purification.

■ ABBREVIATIONS

ARA, arachidonic acid; FTDP-17, frontotemporal dementia with parkinsonism linked to chromosome 17; LLS, right-angle laser light scattering; MTBR, microtubule-binding repeat region; ThS, thioflavin S; WT, wild type.

REFERENCES

(1) Weingarten, M. D., Lockwood, A. H., Hwo, S. Y., and Kirschner, M. W. (1975) A protein factor essential for microtubule assembly. *Proc. Natl. Acad. Sci. U.S.A. 72*, 1858−1862.

(2) Gauthier-Kemper, A., Weissmann, C., Golovyashkina, N., Sebo-Lemke, Z., Drewes, G., Gerke, V., Heinisch, J. J., and Brandt, R. (2011) The frontotemporal dementia mutation R406W blocks tau's interaction with the membrane in an annexin A2-dependent manner. *J. Cell Biol. 192*, 647−661.

(3) Lee, G., Newman, S. T., Gard, D. L., Band, H., and Panchamoorthy, G. (1998) Tau interacts with src-family non-receptor tyrosine kinases. *J. Cell Sci. 111*, 3167−3177.

(4) Chen, J., Kanai, Y., Cowan, N. J., and Hirokawa, N. (1992) Projection domains of MAP2 and tau determine spacings between microtubules in dendrites and axons. *Nature 360*, 674−677.

(5) Brandt, R., Leger, J., and Lee, G. (1995) Interaction of tau with the neural plasma membrane mediated by tau's amino-terminal projection domain. *J. Cell Biol. 131*, 1327−1340.

(6) Goedert, M., Spillantini, M. G., Potier, M. C., Ulrich, J., and Crowther, R. A. (1989) Cloning and sequencing of the cDNA encoding an isoform of microtubule-associated protein tau containing four tandem repeats: Differential expression of tau protein mRNAs in human brain. *EMBO J. 8*, 393−399.

(7) Himmler, A., Drechsel, D., Kirschner, M. W., and Martin, D. W., Jr. (1989) Tau consists of a set of proteins with repeated C-terminal microtubule-binding domains and variable N-terminal domains. *Mol. Cell. Biol. 9*, 1381−1388.

(8) Goode, B. L., and Feinstein, S. C. (1994) Identification of a novel microtubule binding and assembly domain in the developmentally regulated inter-repeat region of tau. *J. Cell Biol. 124*, 769−782.

(9) Wischik, C. M., Novak, M., Thogersen, H. C., Edwards, P. C., Runswick, M. J., Jakes, R., Walker, J. E., Milstein, C., Roth, M., and Klug, A. (1988) Isolation of a fragment of tau derived from the core of the paired helical filament of Alzheimer disease. *Proc. Natl. Acad. Sci. U.S.A. 85*, 4506−4510.

(10) Gamblin, T. C., Berry, R. W., and Binder, L. I. (2003) Modeling tau polymerization in vitro: A review and synthesis. *Biochemistry 42*, 15009−15017.

(11) von Bergen, M., Friedhoff, P., Biernat, J., Heberle, J., and Mandelkow, E. (2000) Assembly of tau protein into Alzheimer paired helical filaments depends on a local sequence motif (306VQIVYK311) forming β structure. *Proc. Natl. Acad. Sci. U.S.A. 97*, 5129−5134.

(12) Giannetti, A. M., Lindwall, G., Chau, M. F., Radeke, M. J., Feinstein, S. C., and Kohlstaedt, L. A. (2000) Fibers of tau fragments, but not full length tau, exhibit a cross β-structure: Implications for the formation of paired helical filaments. *Protein Sci. 9*, 2427−2435.

(13) Li, L., von Bergen, M., Mandelkow, E. M., and Mandelkow, E. (2002) Structure, stability, and aggregation of paired helical filaments from tau protein and FTDP-17 mutants probed by tryptophan scanning mutagenesis. *J. Biol. Chem. 277*, 41390−41400.

(14) Sawaya, M. R., Sambashivan, S., Nelson, R., Ivanova, M. I., Sievers, S. A., Apostol, M. I., Thompson, M. J., Balbirnie, M., Wiltzius, J. J., McFarlane, H. T., Madsen, A. O., Riekel, C., and Eisenberg, D. (2007) Atomic structures of amyloid cross-β spines reveal varied steric zippers. *Nature 447*, 453−457.

(15) von Bergen, M., Barghorn, S., Biernat, J., Mandelkow, E. M., and Mandelkow, E. (2005) Tau aggregation is driven by a transition from random coil to β sheet structure. *Biochim. Biophys. Acta 1739*, 158−166.

(16) King, M. E., Ahuja, V., Binder, L. I., and Kuret, J. (1999) Ligand-dependent tau filament formation: Implications for Alzheimer's disease progression. *Biochemistry 38*, 14851−14859.

(17) Congdon, E. E., Kim, S., Bonchak, J., Songrug, T., Matzavinos, A., and Kuret, J. (2008) Nucleation-dependent tau filament formation: The importance of dimerization and an estimation of elementary rate constants. *J. Biol. Chem. 283*, 13806−13816.

(18) Lee, V. M., Goedert, M., and Trojanowski, J. Q. (2001) Neurodegenerative tauopathies. *Annu. Rev. Neurosci. 24*, 1121−1159.

(19) Sergeant, N., Delacourte, A., and Buee, L. (2005) Tau protein as a differential biomarker of tauopathies. *Biochim. Biophys. Acta 1739*, 179−197.

(20) Hutton, M., Lendon, C. L., Rizzu, P., Baker, M., Froelich, S., Houlden, H., Pickering-Brown, S., Chakraverty, S., Isaacs, A., Grover, A., Hackett, J., Adamson, J., Lincoln, S., Dickson, D., Davies, P., Petersen, R. C., Stevens, M., de Graaff, E., Wauters, E., van Baren, J., Hillebrand, M., Joosse, M., Kwon, J. M., Nowotny, P., Heutink, P., et al. (1998) Association of missense and 5′-splice-site mutations in tau with the inherited dementia FTDP-17. *Nature 393*, 702−705.

(21) Spillantini, M. G., Murrell, J. R., Goedert, M., Farlow, M. R., Klug, A., and Ghetti, B. (1998) Mutation in the tau gene in familial multiple system tauopathy with presenile dementia. *Proc. Natl. Acad. Sci. U.S.A. 95*, 7737−7741.

(22) Arrasate, M., Perez, M., Armas-Portela, R., and Avila, J. (1999) Polymerization of tau peptides into fibrillar structures. The effect of FTDP-17 mutations. *FEBS Lett. 446*, 199−202.

(23) Barghorn, S., Zheng-Fischhofer, Q., Ackmann, M., Biernat, J., von Bergen, M., Mandelkow, E. M., and Mandelkow, E. (2000) Structure, microtubule interactions, and paired helical filament aggregation by tau mutants of frontotemporal dementias. *Biochemistry 39*, 11714−11721.

(24) DeTure, M., Ko, L. W., Yen, S., Nacharaju, P., Easson, C., Lewis, J., van Slegtenhorst, M., Hutton, M., and Yen, S. H. (2000) Missense tau mutations identified in FTDP-17 have a small effect on tau-microtubule interactions. *Brain Res. 853*, 5−14.

(25) Gamblin, T. C., King, M. E., Dawson, H., Vitek, M. P., Kuret, J., Berry, R. W., and Binder, L. I. (2000) In vitro polymerization of tau protein monitored by laser light scattering: Method and application to the study of FTDP-17 mutants. *Biochemistry 39*, 6136−6144.

(26) Nacharaju, P., Lewis, J., Easson, C., Yen, S., Hackett, J., Hutton, M., and Yen, S. H. (1999) Accelerated filament formation from tau protein with specific FTDP-17 missense mutations. *FEBS Lett. 447*, 195−199.

(27) Nagiec, E. W., Sampson, K. E., and Abraham, I. (2001) Mutated tau binds less avidly to microtubules than wildtype tau in living cells. *J. Neurosci. Res. 63*, 268−275.

(28) Sahara, N., Tomiyama, T., and Mori, H. (2000) Missense point mutations of tau to segregate with FTDP-17 exhibit site-specific effects on microtubule structure in COS cells: A novel action of R406W mutation. *J. Neurosci. Res. 60*, 380−387.

(29) Vogelsberg-Ragaglia, V., Bruce, J., Richter-Landsberg, C., Zhang, B., Hong, M., Trojanowski, J. Q., and Lee, V. M. (2000) Distinct FTDP-17 missense mutations in tau produce tau aggregates and other pathological phenotypes in transfected CHO cells. *Mol. Biol. Cell 11*, 4093−4104.

(30) Yen, S. H., Hutton, M., DeTure, M., Ko, L. W., and Nacharaju, P. (1999) Fibrillogenesis of tau: Insights from tau missense mutations in FTDP-17. *Brain Pathol. 9*, 695−705.

(31) Alonso Adel, C., Mederlyova, A., Novak, M., Grundke-Iqbal, I., and Iqbal, K. (2004) Promotion of hyperphosphorylation by frontotemporal dementia tau mutations. *J. Biol. Chem. 279*, 34873−34881.

(32) Kraemer, B. C., Zhang, B., Leverenz, J. B., Thomas, J. H., Trojanowski, J. Q., and Schellenberg, G. D. (2003) Neurodegeneration and defective neurotransmission in a *Caenorhabditis elegans* model of tauopathy. *Proc. Natl. Acad. Sci. U.S.A. 100*, 9980−9985.

(33) Shulman, J. M., and Feany, M. B. (2003) Genetic modifiers of tauopathy in *Drosophila*. *Genetics 165*, 1233−1242.

(34) Tanemura, K., Akagi, T., Murayama, M., Kikuchi, N., Murayama, O., Hashikawa, T., Yoshiike, Y., Park, J. M., Matsuda, K., Nakao, S., Sun, X., Sato, S., Yamaguchi, H., and Takashima, A. (2001) Formation of filamentous tau aggregations in transgenic mice expressing V337M human tau. *Neurobiol. Dis. 8*, 1036−1045.

(35) Delobel, P., Flament, S., Hamdane, M., Jakes, R., Rousseau, A., Delacourte, A., Vilain, J. P., Goedert, M., and Buee, L. (2002) Functional characterization of FTDP-17 tau gene mutations through their effects on *Xenopus* oocyte maturation. *J. Biol. Chem. 277*, 9199−9205.

(36) Lee, V. M., Kenyon, T. K., and Trojanowski, J. Q. (2005) Transgenic animal models of tauopathies. *Biochim. Biophys. Acta 1739*, 251−259.
(37) Rankin, C. A., and Gamblin, T. C. (2008) Assessing the toxicity of tau aggregation. *J. Alzheimer's Dis. 14*, 411−416.
(38) Gamblin, T. C., Berry, R. W., and Binder, L. I. (2003) Tau polymerization: Role of the amino terminus. *Biochemistry 42*, 2252−2257.
(39) Goedert, M., and Jakes, R. (2005) Mutations causing neurodegenerative tauopathies. *Biochim. Biophys. Acta 1739*, 240−250.
(40) Hasegawa, M., Smith, M. J., and Goedert, M. (1998) Tau proteins with FTDP-17 mutations have a reduced ability to promote microtubule assembly. *FEBS Lett. 437*, 207−210.
(41) Wszolek, Z. K., Slowinski, J., Golan, M., and Dickson, D. W. (2005) Frontotemporal dementia and parkinsonism linked to chromosome 17. *Folia Neuropathol. 43*, 258−270.
(42) Kyte, J., and Doolittle, R. F. (1982) A simple method for displaying the hydropathic character of a protein. *J. Mol. Biol. 157*, 105−132.
(43) Chou, P. Y., and Fasman, G. D. (1974) Conformational parameters for amino acids in helical, β-sheet, and random coil regions calculated from proteins. *Biochemistry 13*, 211−222.
(44) Chiti, F., Stefani, M., Taddei, N., Ramponi, G., and Dobson, C. M. (2003) Rationalization of the effects of mutations on peptide and protein aggregation rates. *Nature 424*, 805−808.
(45) Rankin, C. A., Sun, Q., and Gamblin, T. C. (2005) Pseudo-phosphorylation of tau at Ser202 and Thr205 affects tau filament formation. *Brain Res. Mol. Brain Res. 138*, 84−93.
(46) Morris, A. M., Watzky, M. A., Agar, J. N., and Finke, R. G. (2008) Fitting neurological protein aggregation kinetic data via a 2-step, minimal/"Ockham's razor" model: The Finke-Watzky mechanism of nucleation followed by autocatalytic surface growth. *Biochemistry 47*, 2413−2427.
(47) Sun, Q., and Gamblin, T. C. (2009) Pseudohyperphosphorylation causing AD-like changes in tau has significant effects on its polymerization. *Biochemistry 48*, 6002−6011.
(48) Combs, B., Voss, K., and Gamblin, T. C. (2011) Pseudohyperphosphorylation has differential effects on polymerization and function of tau isoforms. *Biochemistry 50*, 9446−9456.
(49) Carlson, S. W., Branden, M., Voss, K., Sun, Q., Rankin, C. A., and Gamblin, T. C. (2007) A complex mechanism for inducer mediated tau polymerization. *Biochemistry 46*, 8838−8849.
(50) Friedhoff, P., Schneider, A., Mandelkow, E. M., and Mandelkow, E. (1998) Rapid assembly of Alzheimer-like paired helical filaments from microtubule-associated protein tau monitored by fluorescence in solution. *Biochemistry 37*, 10223−10230.
(51) Li, W., and Lee, V. M. (2006) Characterization of two VQIXXK motifs for tau fibrillization in vitro. *Biochemistry 45*, 15692−15701.
(52) von Bergen, M., Barghorn, S., Li, L., Marx, A., Biernat, J., Mandelkow, E. M., and Mandelkow, E. (2001) Mutations of tau protein in frontotemporal dementia promote aggregation of paired helical filaments by enhancing local β-structure. *J. Biol. Chem. 276*, 48165−48174.
(53) Jeganathan, S., Hascher, A., Chinnathambi, S., Biernat, J., Mandelkow, E. M., and Mandelkow, E. (2008) Proline-directed pseudo-phosphorylation at AT8 and PHF1 epitopes induces a compaction of the paperclip folding of Tau and generates a pathological (MC-1) conformation. *J. Biol. Chem. 283*, 32066−32076.
(54) Jeganathan, S., von Bergen, M., Brutlach, H., Steinhoff, H. J., and Mandelkow, E. (2006) Global hairpin folding of tau in solution. *Biochemistry 45*, 2283−2293.
(55) Mirra, S. S., Murrell, J. R., Gearing, M., Spillantini, M. G., Goedert, M., Crowther, R. A., Levey, A. I., Jones, R., Green, J., Shoffner, J. M., Wainer, B. H., Schmidt, M. L., Trojanowski, J. Q., and Ghetti, B. (1999) Tau pathology in a family with dementia and a P301L mutation in tau. *J. Neuropathol. Exp. Neurol. 58*, 335−345.
(56) Liu, F., and Gong, C. X. (2008) Tau exon 10 alternative splicing and tauopathies. *Mol. Neurodegener. 3*, 8.
(57) LeBoeuf, A. C., Levy, S. F., Gaylord, M., Bhattacharya, A., Singh, A. K., Jordan, M. A., Wilson, L., and Feinstein, S. C. (2008) FTDP-17 mutations in Tau alter the regulation of microtubule dynamics: An "alternative core" model for normal and pathological Tau action. *J. Biol. Chem. 283*, 36406−36415.
(58) van Herpen, E., Rosso, S. M., Serverijnen, L. A., Yoshida, H., Breedveld, G., van de Graaf, R., Kamphorst, W., Ravid, R., Willemsen, R., Dooijes, D., Majoor-Krakauer, D., Kros, J. M., Crowther, R. A., Goedert, M., Heutink, P., and van Swieten, J. C. (2003) Variable phenotypic expression and extensive tau pathology in two families with the novel tau mutation L315R. *Ann. Neurol. 54*, 573−581.
(59) Barghorn, S., Zheng-Fischhofer, Q., Ackmann, M., Biernat, J., von Bergen, M., and Mandelkow, E. (2000) Structure, microtubule interactions, and paired helical filament aggregation by tau mutants of frontotemporal dementias. *Biochemistry 39*, 11714−11721.
(60) Grover, A., DeTure, M., Yen, S. H., and Hutton, M. (2002) Effects on splicing and protein function of three mutations in codon N296 of tau in vitro. *Neurosci. Lett. 323*, 33−36.
(61) Neumann, M., Schulz-Schaeffer, W., Crowther, R. A., Smith, M. J., Spillantini, M. G., Goedert, M., and Kretzschmar, H. A. (2001) Pick's disease associated with the novel Tau gene mutation K369I. *Ann. Neurol. 50*, 503−513.